Lab on a Chip

PAPER

View Article Online
View Journal

Cite this: DOI: 10.1039/d2lc01070d

Mitigating neutrophil trafficking and cardiotoxicity with DS–IkL in a microphysiological system of a cytokine storm†

Venktesh S. Shirure, Sergey Yechikov, Bhupinder S. Shergill, Tima Dehghani, Anton V. Block, Harkanwalpreet Sodhi, Alyssa Panitch‡ and Steven C. George‡*

A feature of severe COVID-19 is the onset of an acute and intense systemic inflammatory response referred to as the "cytokine storm". The cytokine storm is characterized by high serum levels of inflammatory cytokines and the subsequent transport of inflammatory cells to damaging levels in vital organs (*e.g.*, myocarditis). Immune trafficking and its effect on underlying tissues (*e.g.*, myocardium) are challenging to observe at a high spatial and temporal resolution in mouse models. In this study, we created a vascularized organ-on-a-chip system to mimic cytokine storm-like conditions and tested the effectiveness of a novel multivalent selectin-targeting carbohydrate conjugate (composed of DS – dermatan sulfate and IkL – a selectin-binding peptide, termed DS–IkL) in blocking infiltration of polymorphonuclear leukocytes (PMN). Our data shows that cytokine storm-like conditions induce endothelial cells to produce additional inflammatory cytokines and facilitate infiltration of PMNs into tissue. Treatment of tissues with DS–IkL (60 μM) reduced PMN accumulation in the tissue by >50%. We then created cytokine storm-like conditions in a vascularized cardiac tissue-chip and found that PMN infiltration increases the spontaneous beating rate of the cardiac tissue, and this effect is eliminated by treatment with DS–IkL (60 μM). In summary, we demonstrate the utility of an organ-on-a-chip platform to mimic COVID-19 related cytokine storm and that blocking leukocyte infiltration with DS–IkL could be a viable strategy to mitigate associated cardiac complications.

Received 18th November 2022,
Accepted 30th May 2023

DOI: 10.1039/d2lc01070d

rsc.li/loc

Introduction

COVID-19, the clinical disease caused by the SARS-CoV-2 coronavirus, was classified by the World Health Organization as a pandemic in March 2020 and has impacted human health and the economy on a global scale. A feature of severe disease, which is responsible for a majority of COVID-19 deaths, is the onset of an acute and intense systemic inflammatory response referred to as the "cytokine storm".[1,2] The cytokine storm is characterized by high serum levels of a slew of inflammatory cytokines (*e.g.*, IL-6, TNFα, IL-1β, and IFNγ). This is generally thought to be initiated by the release of TNFα and IL-1β from respiratory epithelial cells which can induce nuclear translocation of NF-κB of neighboring cells leading to the expression of many additional cytokines such as IL-6 and IFNγ.[3,4] The cytokine storm can lead to enhanced permeability of the vascular endothelium and the subsequent transport of inflammatory cells and cytokines to damaging levels in vital organs (*e.g.*, myocarditis).[5,6] Indeed, cardiac arrhythmias are a major source of morbidity and mortality (44–60%) associated with COVID-19.[7–10] Reports have indicated that 20–22% of hospitalized patients with SARS-CoV-2 experience cardiac injury, and these patients suffer a staggering 50% mortality rate, more than an order of magnitude higher than those patients without cardiac injury.[7,11]

Treatments neutralizing the excess inflammatory cytokines (*e.g.*, anti-IL-6) have been beneficial for COVID-19 patients,[12] but treatments directly inhibiting the extravasation of immune cells into organs, a source of additional cytokines, have thus far not been tested. The extravasation of circulating immune cells into inflamed tissues involves a cascade of events, starting with rolling and arrest on the endothelium, followed by extravasation, migration, and elicitation of the effector function in the tissue. An attractive strategy to limit extravasation is to reduce initial rolling and attachment of immune cells. This process is partly mediated by endothelial E-selectin.

Department of Biomedical Engineering, University of California, Davis, 451 E. Health Sciences Drive, Room 2315, Davis, CA 95616, USA.
E-mail: scgeorge@ucdavis.edu; Tel: +1 530 752 9978

† Electronic supplementary information (ESI) available. See DOI: https://doi.org/10.1039/d2lc01070d

‡ Contributed equally as co-senior authors.

Drugs targeting E-selectin have been developed but face significant challenges including: 1) redundant endothelial adhesion molecules (*e.g.*, VCAM-1, ICAM-1); 2) drug instability in an inflammatory environment; and 3) on-target off-site toxicities.[13–15] We have developed a multivalent selectin-targeting carbohydrate conjugate (termed DS–IkL)[16] that is comprised of: 1) a natural glycosaminoglycan-derived backbone (DS – dermatan sulfate), normally present in the endothelial glycocalyx; and 2) a selectin-binding peptide (GRGsIkLLpOR – abbreviated IkL) consisting of D-amino acids to increase the enzymatic stability in inflammatory environments. The selectin binding peptide provides specificity of DS–IkL to bind injured, damaged, or inflamed endothelium. The large complex of this drug effectively creates an "umbrella" that is tethered to E-selectin masking other adhesion molecules and thus limiting immune cell attachment. Significantly, DS–IkL has been shown to inhibit both platelet activation and neutrophil trafficking from the circulation into damaged myocardium *in vivo*,[16] and is uniquely positioned to mitigate neutrophil extravasation, and thus cytokine storm.

Immune trafficking and its effect on underlying tissues (*e.g.*, myocardium) are challenging to observe at high spatial and temporal resolution in mouse models. Moreover, the immunology and biology of humans is inherently different from mice. Organ-on-a-chip technologies create 3D functional tissue mimics from human cells offering an intriguing alternative model system. Our lab has created organ-on-a-chip technologies that include functional microvasculature with physiological shear, physiological interstitial flow, bone marrow niches, cardiac, as well as solid tumor tissue mimics.[17–21] These platforms are optically clear providing simple and reproducible observation at cellular and subcellular levels without perturbing the tissue microenvironment.

In this study, we have created an organ-on-a-chip system to observe leukocyte trafficking (tethering, rolling, arrest, and tissue infiltration) into a cardiac microenvironment ('cardiac tissue-chip') under conditions that mimic the cytokine storm of COVID-19. In particular we utilize a range of concentrations of IL-1β and TNFα as the initial inflammatory stimulus,[3,4] that include those reported in the serum of patients with severe COVID-19 (only 100 pg ml^{-1} (ref. 22)) and as high as 10 ng ml^{-1}, consistent with many prior *in vitro* experiments.[23–25] We then use the system to test the efficacy of DS–IkL to inhibit neutrophil trafficking. Our data demonstrate that the initial stimulus of IL-1β and TNFα at concentrations as low as 100 pg ml^{-1} lead to the production of IL-6 and IFNγ by the endothelium, and neutrophil extravasation is enhanced at these levels of cytokines present in the serum of patients with COVID-19. Furthermore, neutrophil extravasation enhances the spontaneous beat rate of the cardiomyocytes, and this effect is attenuated in the presence of DS–IkL.

Materials and methods

Cell culture

Endothelial colony forming cell-derived endothelial cells (**ECs**) were derived from cord blood as detailed previously.[17,26] The ECs were grown up to seven passages in fully supplemented endothelial growth medium (**EGM**-2; Lonza). Adult human atrial cardiac fibroblasts (**CF**s) were purchased from Cell Applications and were cultured in recommended media (Cell Applications). The human induced pluripotent stem cell line (**hiPSC**), WTC11, with integrated GCaMP6 reporter at the AAVS1 safe harbor locus was obtained from the Gladstone Institute Stem Cell Core. The fluorescence created by the GCaMP6 reporter facilitates monitoring of intracellular calcium transients. The hiPSCs were cultured in mTeSR1 (Stem Cell Technologies) on growth-factor reduced Matrigel (Corning) and passaged using ReLeSR (Stem Cell Technologies). One day before initiating differentiation, the hiPSCs were dissociated using Accutase dissociation reagent (ThermoFisher) and plated in 12-well plates, and allowed to grow to 80% confluency. Details of the hiPSC differentiation into atrial-like cardiomyocytes (**hiPS-aCM**) have been previously published,[18,27] and only the salient features are presented here. On the day of differentiation, media was changed to RPMI 1640 with L-glutamine (ThermoFisher) containing B-27 supplement without insulin (ThermoFisher). Fully confluent hiPSCs were treated with 12 mM glycogen synthase kinase (GSK)-3 inhibitor – CHIR99021 (LC Laboratories) for 24 hours. On day 3, cells were treated with 5 mM Wnt inhibitor, IWP-2 (Tocris) and 1 μM retinoic acid (RA) (Sigma) for 48 hours. After day 7, hiPS-derived cardiomyocytes were maintained in RPMI 1640 with L-glutamine and B-27 supplement with insulin (ThermoFisher). Cells were maintained and allowed to differentiate into (hiPS-aCM) until day 60, and then were cryopreserved for a future use.

Polymorphonuclear (PMN) cell isolation and activation

PMNs were isolated from human donor whole blood using EasySep Direct Human Neutrophil Isolation Kit (STEMCELL Technologies) according to manufacturer instructions using the EasySep magnet. The study was approved by the Institutional Review Board (IRB) at the University of California, Davis, followed all institutional guidelines for human subjects research, and informed consent was obtained from all participating subjects. Following PMN labelling (see fluorescence labelling section below), PMNs were activated in EGM-2 without VEGF and FGF, with the addition of TNFα and IL-1β at 100 pg ml^{-1}, consistent with serum levels of patients with severe COVID-19,[22] and incubated for 30 minutes at 37 °C.

Fluorescence labelling of cells

The ECs and PMNs were labelled with CellTracker Orange CMRA and CellTracker Violet BMQC, respectively, following

the manufacture recommended protocol. Briefly, a 3 μM solution of the dye was prepared in DPBS and the cells were incubated at 0.5 million per mL at 37 °C for 30 min. The cells were then washed twice with DPBS and prepared for loading.

Microfabrication

The process of microfabrication is described in detail elsewhere.[20] In short, a SU8 master mold was prepared using photolithography. The microdevice was created by casting polydimethylsiloxane (PDMS), which was prepared by mixing Sylgard® 184 silicone elastomer base and curing agent (both Dow Corning, Midland, MI) in a 10 : 1 ratio, on the SU-8 master molds. The device was peeled off the master mold and then bonded to a flat PDMS sheet using air plasma. The bottoms of cryovials were cut off to create cylindrical source and sink reservoirs, which were attached the inlet and outlet ports of ch3 (Fig. 1A) of each device using PDMS as glue.

Device design, cell loading, tissue creation

Our model of the vascularized cardiac tissue is created using a microfluidic device with five parallel fluidic lines (Fig. 1B): 1) the central channel (ch1) is lined with a monolayer of endothelial cells to create a vessel-like compartment; 2) adjacent to the central channel are channels (ch2A and ch2B) that are loaded with hydrogel (fibrin) that may or may not contain hiPS-aCM and CFs to create the cardiac microenvironment of the cardiac tissue-chip; and 3) the outer most channels (ch3A and ch3B) which serve to collect interstitial flow through the tissue compartments.

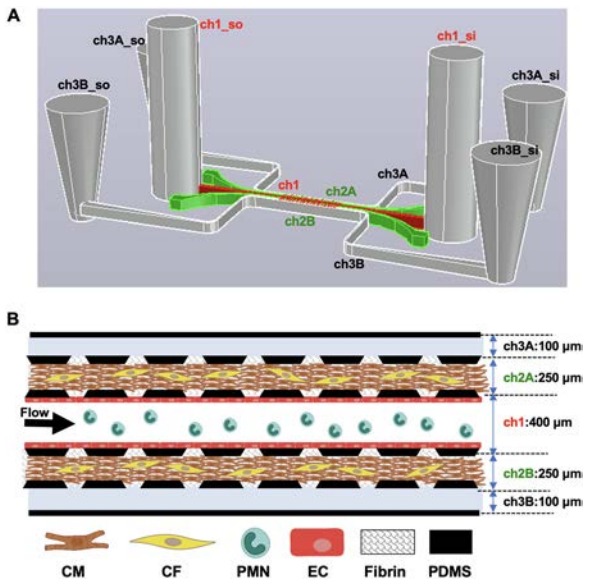

Fig. 1 A vascularized cardiac tissue-chip design to observe attachment and extravasation of circulating cells in a tissue microenvironment under physiological flow conditions. A) The device design consists of five parallel channels (ch1, ch2A, ch2B, ch3A, and ch3B). Cylindrical cryovials act as a source (ch1_so) and a sink (ch1_si) for ch1 (red) and micropipettes act as sinks and sources to ch3 (grey). B) A schematic of the device shown from a top-view. Ch2 are loaded with a mixture of hiPS-aCM, CFs and fibrin or only fibrin, and ch1 is coated with ECs to mimic a vessel. The tissues are maintained and treated with cytokines and/or drugs, followed by perfusing PMNs through ch1 at physiologic shear.

A fibrin-based tissue (with or without hiPS-aCM and CF) was prepared by mixing bovine fibrinogen (Sigma-Aldrich, St. Louis, MO) and bovine plasma thrombin (Sigma-Aldrich). Fibrinogen solution was prepared at 10 mg ml^{-1} in DPBS without ions, incubated overnight at 37 °C, and filtered using low protein binding 0.22 μm syringe filters (Millipore), and thrombin was prepared at 50 U ml^{-1}. 15 μL of fibrinogen and 0.9 μL of thrombin were mixed and quickly introduced into ch2 of the device (Fig. 1A). The tissue was allowed to gel for 30 min, and the central chamber (ch1) was coated with 15 μL of 0.2% gelatin for 30 min. The chamber was then perfused with ECs at 25 million per mL concentration. The cells were allowed to attach to the surface for 4 h. Unattached cells were flushed and the devices were fed through ch1 with EGM media without VEGF and FGF. Some media was also perfused through ch3A and ch3B to create a hydrostatic pressure head of about 10 mm H_2O across the tissue, which creates a physiological interstitial fluid velocity through the tissue.[18,20] The media was replaced daily for 48 h to allow the endothelium to fully form; the devices were then used for perfusion experiments.

The vascularized cardiac tissue-chip was prepared by first creating and developing the cardiac tissue in ch2 for five days, and then creating the endothelial vessel in ch1. To create the cardiac tissue, the surface of the tissue chambers (ch2A and ch2B) was first coated with Matrigel diluted at 1 : 100 in RPMI media. Next, cryopreserved hiPS-aCM[28] and CFs were thawed, washed with calcium/magnesium free PBS, and mixed with fibrinogen (40 mg mL^{-1}) and the resulting mixture was mixed with thrombin (4 U mL^{-1}) to yield total concentration of cells = 4×10^8 mL^{-1} (hiPS-aCM : CF = 2.4 : 1), and fibrinogen concentration of 10 mg mL^{-1}. The loaded tissue was allowed to settle for about 30 min. Next, the central chamber (ch1) of the device was treated with 1 : 100 Matrigel solution in RPMI for 30 min and finally the devices were fed with cardiomyocyte maintenance media. These tissues were allowed to develop for 5 days, and then ECs were loaded into ch1 following the EC-coating protocol described above. After EC-coating, the devices were maintained with 1 : 1 mixture of EC/cardiomyocyte media.

Device treatments mimicking cytokine storm

On the day of PMN perfusion, the tissues were treated with IL-1β and TNFα for 4 h, as the initial stimulus of cytokine storm-like conditions,[3,4] then incubated with media containing DS–IkL or no-drug. The concentration of IL-1β and TNFα varied from as low as 100 pg ml^{-1} consistent with serum levels of patients with severe COVID-19 (ref. 22) to as high as 10 ng ml^{-1} consistent with many prior *in vitro* experiments.[23–25] After 1 h, the tissue-chips were perfused with 1 mL of PMN suspended at 1×10^6 cells per mL. For

acellular tissues, PMN perfusion was carried out for 30 min followed by perfusion with cell-free media. For vascularized cardiac tissue-chips, the perfusion was carried out for 4 h. To maintain physiologic flow through the vessel, media collected in the sink of the ch1 was recirculated into the source reservoir every 30 min.

Device imaging and analysis

The microtissues were imaged using FV1200 Fluoview biological confocal laser scanning microscope (Olympus) connected to FV10-ASW image acquisition and analysis software (Olympus). The fluorescent images/videos were acquired to analyze attachment and infiltration of the PMNs. The videos acquired for 2 min at the beginning of the perfusion were used to determine rolling velocity. The ImageJ plugin TrackMate was used to track the position of rolling neutrophils acquired at a frame rate of 2.5 frames per s, similar to methods previously described.[29] Analysis was limited to cells in motion by setting the following tracking criteria: threshold value of 800; spots tracked for 5 or more frames; spot remains in constant motion (average velocity >0.05 um s^{-1}), spot tracking limited to center 80% of frame. Velocity was defined as the average (microns travelled per frame × frame rate) over the number of frames tracked: sqrt[(distance travelled in x direction)^2 + (distance travelled in y direction)^2] × 2.5 frames per s. The still images acquired at the end of perfusion were used to quantify PMN attachment to endothelium and extravasation. For this analysis, the fluorescent images were thresholded to remove background and the area of PMN in ch1 and ch2 was measured using ImageJ. The area of PMNs in ch1 was used to quantify attachment to the endothelium, and the area of PMNs in ch2 was used to quantify the infiltration of PMNs.

The spontaneous beating rate (beats per minute; bpm) of cardiac tissues was counted for 5 min by observing fluorescence from the GCaMP6 reporter. The bpm for each device was normalized to bpm of the same device before PMN perfusion. Line scans of GCaMP6 fluorescence were acquired at high-speed using the resonance scanning mode of the microscope (sampling rate: 63 μs) and were utilized to measure field potential duration and travel time for a wave to propagate through the cardiac tissue. To determine conduction velocity, temporal GCaMP6 fluorescence profiles were extracted from 20 evenly assigned areas along the cardiac tissue chambers (ch2). Field action potential profile, extracted from the first area of the device, was used to estimate the action potential duration (APD80 and APD50).

Vessel permeability assay

The barrier function of the endothelium was characterized by performing permeability measurements as detailed previously.[1,2] Briefly, dextran-FITC (MW = 70 kDa and concentration = 100 μg ml^{-1}) was perfused through the endothelialized central chamber, and time lapse images were recorded using an IX83 motorized inverted microscope (Olympus). The image analysis was performed using ImageJ 1.47 V. The permeability of the vessels was calculated using the following equation:[1]

$$P = \frac{1}{I_0}\frac{\mathrm{d}I}{\mathrm{d}t}\frac{v}{s}$$

where P is permeability (cm s^{-1}), I_0 is fluorescent intensity of filled vessel at $t = 0$, $(\mathrm{d}I/\mathrm{d}t)$ is the rate of change in intensity (s^{-1}) within the region of interest in ch2, v is the volume of the filled vessel (ch1) used to determine I_0; cm^3), s is the surface area of endothelial barrier for transport of dextran (cross-sectional area of the pore between ch1 and ch2 in x–z direction; cm^2).

ELISA

Concentrations of IL-1β, IL-6, TNF-α, and IFNγ in cell media were measured using Meso Scale Diagnostics' V-Plex Human Proinflammatory Panel I (4-plex) electrochemifluorescent ELISA as per manufacturer recommendations. Media samples were not diluted for testing and 2% Tween-20 in phosphate buffered saline was used as wash buffer. All cell media samples were stored at −80 °C until analysis.

Statistics

Statistical analysis was performed using one-way ANOVA and Tukey *post hoc* test for multiple comparisons or Student's *t*-test. All data are presented as the mean ± standard deviation. Results were considered statistically significant for $p < 0.05$.

Results

Physiological model of cytokine storm-like conditions on a chip

First, we performed finite element simulations (COMSOL) to determine the desired pressure distribution to maintain a physiologic shear stress on the endothelial surface. The pressures external to the devices (*e.g.*, loading ports) were established to create a pressure drop from source (so) to sink (si) of ch1 and across ch2 (Fig. 1A and 2A). This pressure profile creates luminal flow (x-direction) in ch1 and interstitial flow (largely in the y-direction) in ch2 (Fig. 2B). The hydrostatic pressure head, ΔP_{ch1} (= $P_{ch1\_so} - P_{ch1\_si}$) decreases over time as the source empties into the sink. The result is a decrease in fluid flow and shear over time. The COMSOL model predicts that it takes about 30 min to reduce ΔP_{ch1} from 20 to 10 mm H_2O (200–100 Pa), and during this window of time the shear stress remains in the physiologic range of shear stress (0.5–6 dyn cm^{-2} or 0.05–0.6 Pa in post-capillary venules where neutrophils extravasate;[30,31] Fig. 2C). We experimentally measured the change in hydrostatic head (difference in height of water column in sink and source of

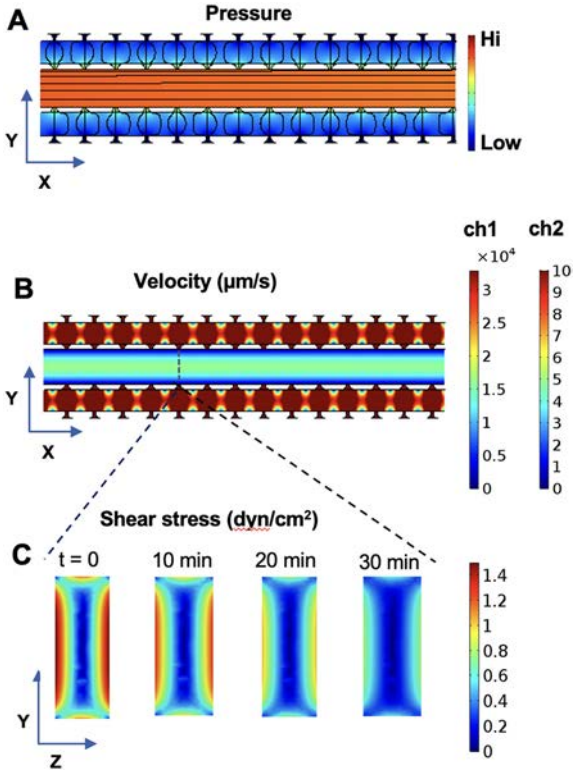

Fig. 2 Hydrostatic pressure gradients drive physiological levels of luminal and interstitial flow. A) COMSOL simulations show pressure distribution in the device. The pressure drop (*x*-direction) in the central channel (ch1) is created by high pressure in the source (left) and low pressure in the sink (right). There is also a pressure drop across (*y*-direction) the side channels (ch2). B) The hydrostatic pressure drop drives fluid through the endothelial cell-lined central channel with high velocity (*x*-direction; ch1) and across (*y*-direction) the gel-filled tissue chambers (ch2) with low velocity. C) The shear stress distribution in the *y*–*z* plane (dotted line in panel B) is shown at various time points. As time progresses the hydrostatic pressure difference between the reservoirs attached to the central chamber decreases. For approximately 30 min a physiological shear stress (>0.5 dyn cm^{-2}) can be achieved over most of the endothelial surface.

ch1) and confirmed that $\Delta P_{ch1} > 10$ mm H_2O for the entire 30 min. The fibrin-filled channels (ch2) offer resistance to fluid flow and the simulations demonstrate that an average pressure drop across ch2 in the *y*-direction of approximately 5 mm H_2O is required to maintain physiological level of interstitial fluid flow velocity (0.1–10 μm s^{-1} (ref. 20, 32 and 33), which is as expected from our previous experimental studies.[17]

To simulate the basic features of cytokine storm, we introduced two well-known inflammatory cytokines, IL-1β and TNFα, which are detected in the serum of COVID-19 patients,[22] and are upstream of IL-6. Given 100 pg mL^{-1} of IL-1β and TNFα has been reported in severe COVID-19 cases,[22] we chose this concentration for simulating the early events[3] of COVID-19 cytokine storm. The ECs stimulated with these cytokines in turn produced TNFα and IL-1β above the stimulus concentration, as well as two additional cytokines (IL-6 and IFNγ; Fig. 3A) reported in severe COVID-19 cases and thought to be central in the pathogenesis.[22,34] Two distinct patterns of cytokine secretion can be observed: 1) the cytokine secretion by ECs proportionately increases with increasing levels of treatment concentrations (TNFα, IL-6, IL-1β); and 2) a step increase in the production of cytokine (IFNγ) at a critical treatment concentration (25 pg mL^{-1}). These data demonstrate that ECs may potentially act as a positive feedback regulator to elevate the level of pro-inflammatory cytokines.

We next characterized the EC coating in ch1, and demonstrated that the ECs formed a confluent monolayer including the pore region of the device (Fig. 3B). To demonstrate barrier function of ECs in the device, we measured the permeability of the endothelialized chamber to 70 kDa dextran (0.8×10^{-5} cm s^{-1}). The permeability was close to permeability of microvessels in other *in vitro* systems.[35,36] When the ECs were treated with IL-1β and TNFα the permeability of the vessel more than quadrupled (3.4×10^{-5} cm s^{-1}; Fig. 3C), consistent with previous reports.[37,38]

Cytokine storm-like conditions enhance PMN accumulation into tissue

Freshly isolated PMNs (>95% pure by flow cytometry; Fig. S1†) from healthy donors were perfused at physiologic flow through the endothelialized central chamber, and we analyzed both the accumulation (total attachment to endothelium plus extravasation or ch1 + ch2) and extravasation alone (ch2). In control devices, which were not coated with ECs, the total accumulation of PMNs was near zero; however, EC-devices treated with IL-1β and TNFα showed a very high level of accumulation and extravasation of PMNs (Fig. 4A–D). There was a significant increase in accumulation and extravasation at 100 pg ml^{-1}, and this was further augmented at 10 ng ml^{-1}, a more typical *in vitro* concentration. Furthermore, at higher treatment concentrations, the proportion of extravasated cells (as a percent of accumulated cells) was higher (two-fold; Fig. 4B). We next activated PMNs by treatment with IL-1β and TNFα (100 pg mL^{-1}). These activated PMNs expressed CD11b (Fig. S1†), a classic PMN activation marker.[39] In general, approximately 3–5% of the accumulated PMNs extravasated into ch2, with no significant difference between non-activated or activated PMNs (Fig. 4A, B, D, and F). Brightfield images of the device confirm confluent monolayer of endothelial cells (Fig. S2†).

DS–IkL inhibits PMN accumulation, rolling, and extravasation

To study the effect of DS–IkL treatment, we treated cytokine-activated tissues with a range of concentrations of DS–IkL and analyzed PMN rolling velocities, accumulation, and extravasation (Fig. 5A). As the treatment concentration of DS–IkL increased, PMN rolling velocity also increased (Fig. 5B and SV1 and SV2†), suggesting that DS–IkL

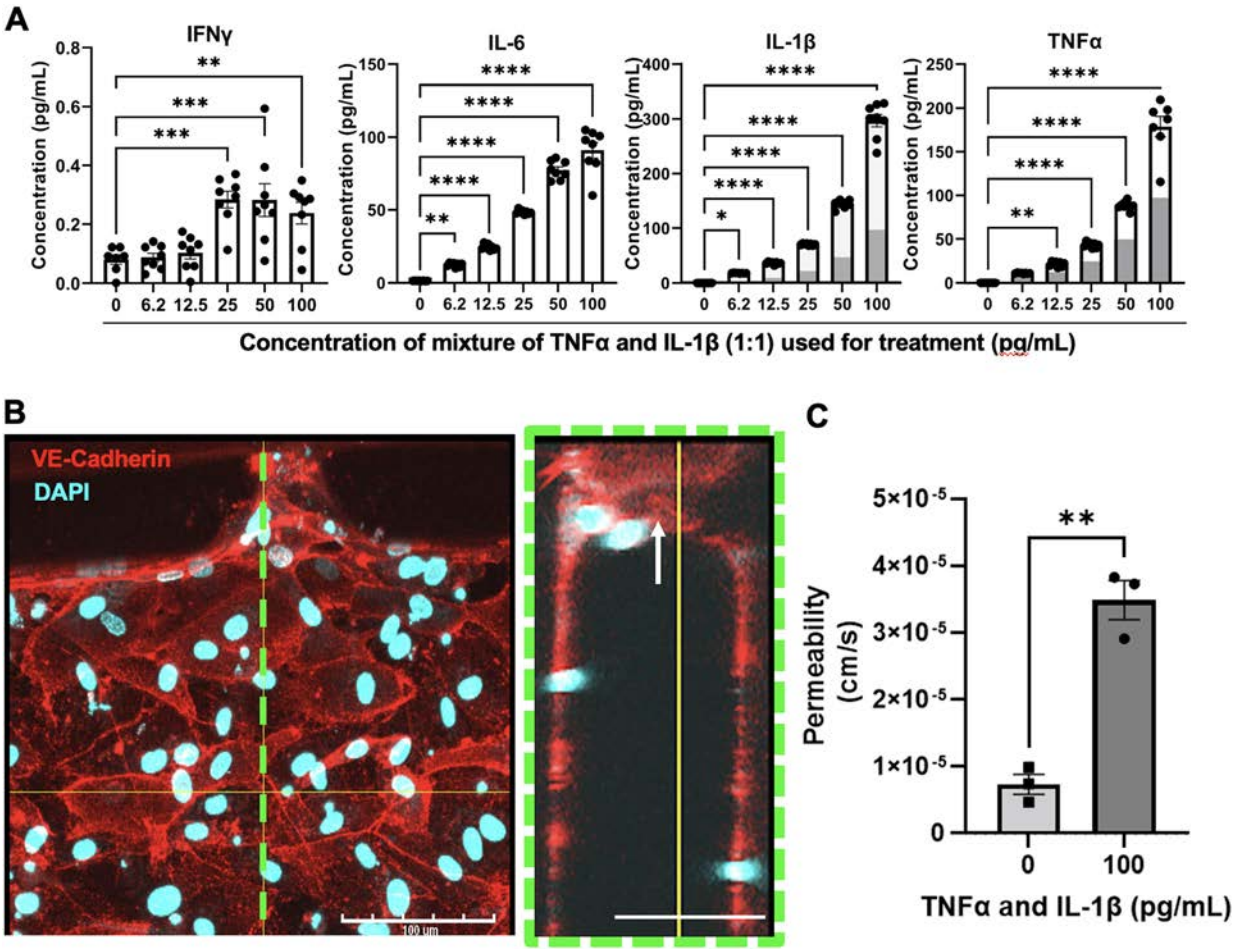

Fig. 3 Endothelial cells amplify COVID-19 relevant inflammatory cytokines and alter permeability in response to TNFα and IL-1β treatment. A) 2D well-plate cultures of endothelial cells were exposed to a range of concentrations of TNFα and IL-1β (1 : 1 mixture) and the supernatants were analyzed for COVID-19 relevant cytokines. The shaded portion of bars (two right panels) indicate contributions from the actual treatment (or stimulus) to the portion of measured cytokines, open portion of bars indicate contribution over and above the stimulus. B) ECs coated in ch1 of the device were stained with VE-cadherin (red) and DAPI (cyan). Scale bar 100 μm. The right panel shows a cross-section of the endothelialized channel along the green dotted line in the left panel. The arrow points to a pore between ch1 and ch2A. C) The permeability of the endothelialized channel to 70 kDa dextran with or without treatment of TNFα and IL-1β.

interferes with the initial interactions between PMN and EC. The activated PMNs, which have integrins in a high affinity state,[39] rolled slower than non-activated PMNs (Fig. 5B). Consistent with rolling velocity, the accumulation of PMNs declined with increasing treatment concentration of DS–IkL (Fig. 5C and E) and accumulation was <50% for treatment concentration of only 0.60 μM (Fig. 5C). When PMNs were also activated, accumulation did not fall below 50% until a DS–IkL concentration of 60 μM. The extravasation of PMNs also decreased by >50% for treatment concentration of 60 μM. The rate of extravasation of both activated and non-activated PMNs decreased with increasing DS–IkL at similar rates (Fig. 5D). Endothelial continuity was not impacted by DS–IkL treatment (Fig. S3†). Together, these data show that the accumulation of PMNs can be significantly reduced (>50%) by DS–IkL, and that activation of PMNs enhances attachment to the endothelium but not extravasation.

DS–IkL mitigates PMN-induced enhanced cardiomyocyte beating rate

To study the effect of cytokine storm-like conditions on cardiomyocytes, we utilized a vascularized cardiac tissue-chip using the same microfluidic device (Fig. 1) and exposed the model system to a set of experimental conditions similar to that described earlier (Fig. 6A). We chose to use activated PMNs in these tissue chips to better recreate the physiological cytokine storm-like environment, as the inflammatory cytokines in the serum of COVID-19 patients are expected to activate the PMNs. The cytokine or drug treatments by themselves did not alter the beating rate, CV, or APD (Fig. 6B–E). However, vascularized cardiac tissue-chips treated with cytokines and PMNs together showed an increased beating rate of ~50% that was statistically significant (Fig. 6B; SV3 and 4 and SV6 and 7†) whereas CV and APD were not impacted (Fig. 6C–E), compared to the

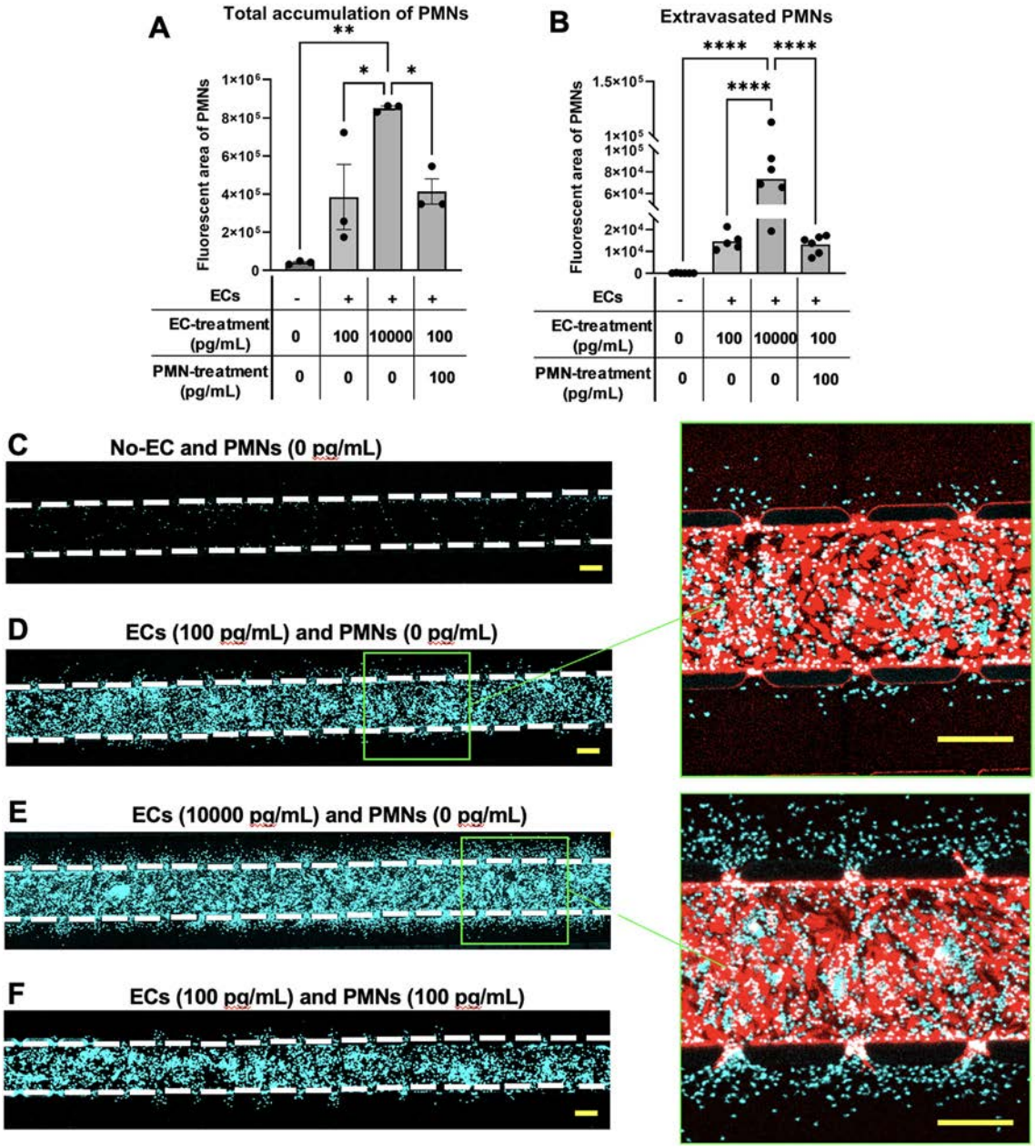

Fig. 4 Cytokine storm-like conditions relevant to COVID-19 facilitate PMN adhesion and extravasation across endothelium in the organ-on-a-chip platform. (A and B) The microfluidic devices were loaded with fibrin in ch2, and ch1 was coated with ECs (+) or not coated with cells (–). The devices were then treated with indicated concentrations TNFα and IL-1β. Finally, PMNs treated with indicated concentrations of the cytokines were perfused through the device and fluorescence area of PMNs was measured to quantify accumulation (total area of PMNs in ch1 and ch2) or extravasation (area of PMNs in ch2A or ch2B). (C–F) Representative images of fluorescently labelled PMNs (cyan) flowed through the vessel (not-shown) under the four conditions in panel A. Dotted white lines indicate separation between vessel (ch1) and fibrin tissue (ch2). Magnified images in the region marked by green box (left panels) are shown (right panels) with endothelial vessel (red) and PMNs. The scale bars indicate 200 μm.

control conditions. The beating rate of the cardiac tissue was reduced to basal levels in the presence of 60 μM DS–IkL (Fig. 6B and SV3–7†).

Discussion

A feature of severe COVID-19 is the onset of an acute and intense systemic inflammatory response referred to as the "cytokine storm".[1] The excess inflammatory cytokines, such as TNFα and IL-1β, released in serum increase expression of adhesion molecules in endothelial cells,[40] activate immune cells[39] and thereby facilitate infiltration of immune cells into underlying tissues to a damaging level. A significant proportion of patients with severe disease experience cardiac injury[7,11] and the myocardium of patients with cardiac complications has been found to have high leukocyte infiltration.[41] Our study utilized a microfluidic model of vascularized cardiac tissue to simulate cytokine storm-like

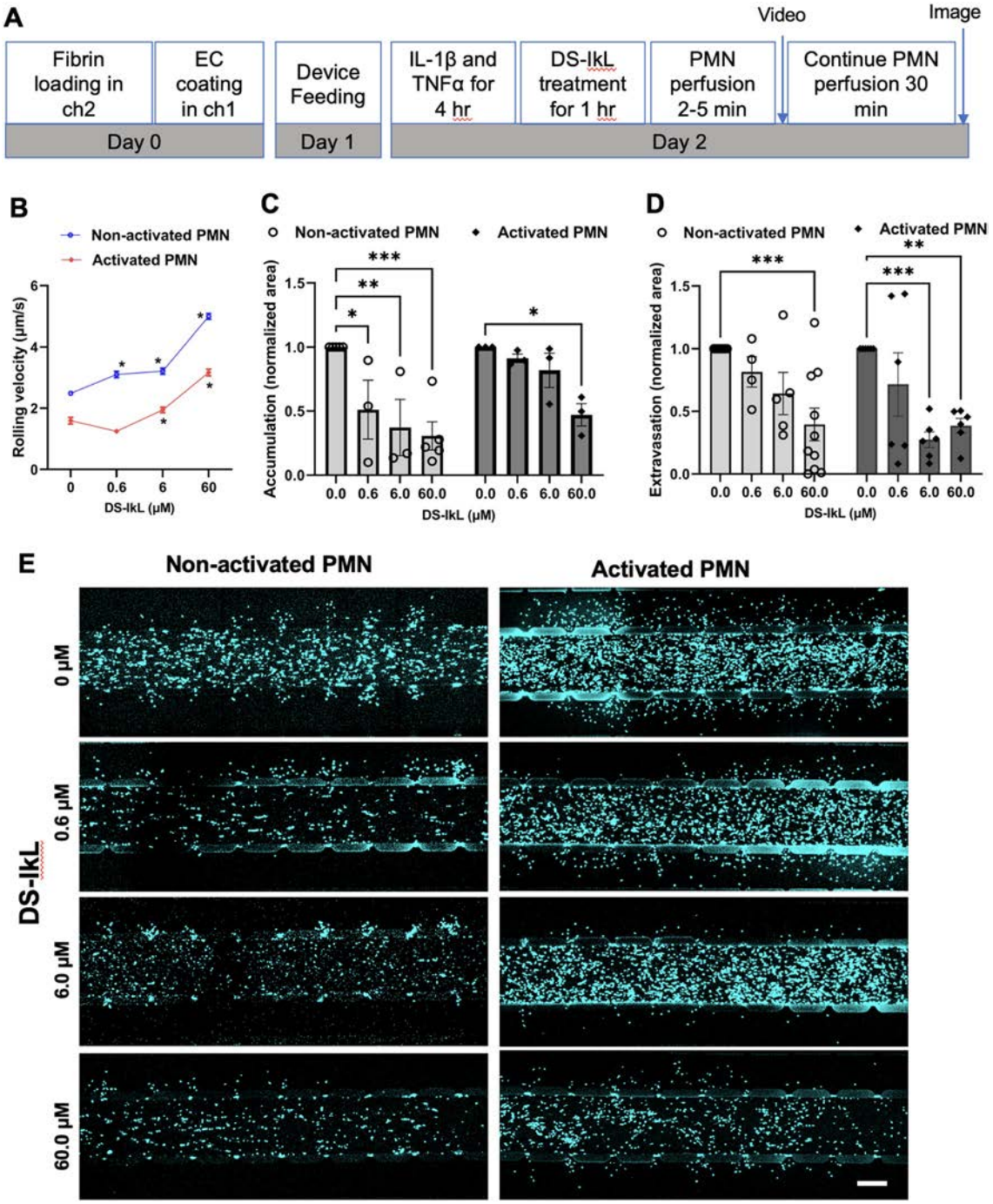

Fig. 5 DS–IkL inhibits adhesion and extravasation of PMNs in the organ-on-a-chip platform. (A) The process flow of the experiment. The microfluidic devices were loaded with fibrin and ECs. The devices were with TNFα and IL-1β (100 pg mL^{-1}) prior to treatment with DS–IkL. Activated PMNs (treated with cytokines) or non-activated PMNs were perfused through ch1 of the device and the timelapse images were recorded to determine rolling velocities. At the end of the perfusion, still images were acquired to quantify extravasation (fluorescence area of PMN in ch2) or accumulation (total fluorescence area in ch1 and ch2). (B) Rolling velocities were computed for a large number of individual PMNs ($n > 400$). (C and D) For each PMN donor, no-drug treatment condition was used to normalize the data. Data are mean ± SEM. (E) Representative images of devices after perfusion of PMNs (cyan) under different drug treatment conditions. The scale bar indicates 200 μm.

conditions associated with COVID-19. Our results demonstrate that levels of TNFα and IL-1β observed in the serum of patients with cytokine storm result in 1) enhanced production of both TNFα and IL-1β, as well as IL-6 and IFNγ; and 2) PMN attachment to the endothelium and extravasation leading to enhanced beating rate of the cardiac tissue. PMN attachment and extravasation was significantly abrogated in the presence of DS–IkL demonstrating DS–IkL may be a useful intervention to mitigate the cardiac effects of cytokine storm.

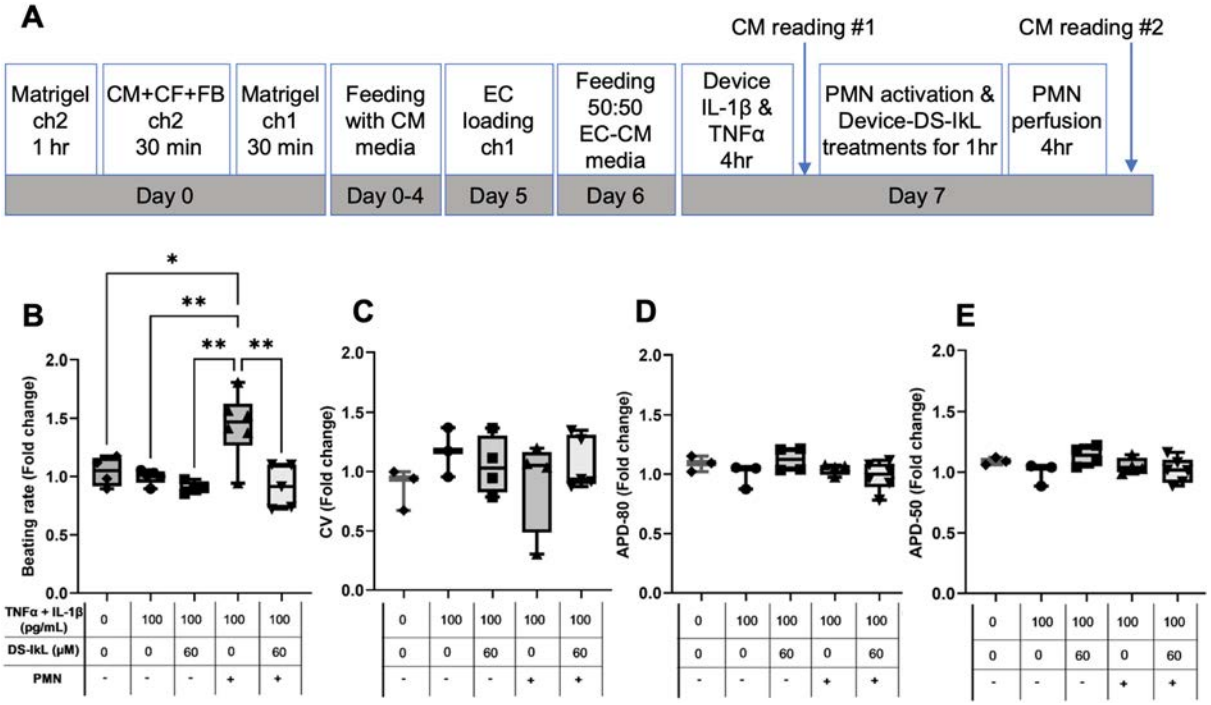

Fig. 6 Cardiac function is impacted by PMN infiltration and DS–IkL alleviates this impact in a vascularized cardiac tissue-chip. (A) The process flow of the device loading and treatments. The microfluidic devices were loaded with CM, CF, and ECs on indicated days and the devices were treated with 100 or 0 pg mL^{-1} of TNFα and IL-1β and 60 or 0 μM of DS–IkL. PMNs were treated with same levels of these cytokines and were perfused through the device. The line scans of CM were recorded, and CM beatings were counted before and after PMN treatment as indicated. (B–E) The cytokine and drug concentrations used for the treatments are indicated. The devices perfused with PMN (+) or not perfused with PMN (–) are as indicated. For each device, the CM reading #2, obtained at the end of the PMN perfusion, was normalized with its own CM reading #1, obtained at the beginning of the treatment. The box shows upper and lower quartiles and the whisker show full range of the data points.

Trafficking of circulating leukocytes into inflamed tissues involves a cascade of events including, initial tethering, rolling and firm arrest on the endothelium, followed by extravasation, migration, and elicitation of the effector function in the tissue. The steps of leukocyte adhesion are mediated by endothelial adhesion molecules, including E- and P-selectin, vascular cell adhesion molecule (VCAM)-1, and intercellular adhesion molecule (ICAM)-1, and their counter receptors on leukocytes, such as P-selectin glycoprotein ligand (PSGL)-1, CD44, and integrins [lymphocyte function-associated antigen (LFA)-1 and very late antigen (VLA)-4]. Mouse models cannot fully represent human immunology; in particular, ECs of mouse and human exhibit major differences in the expression patterns of E- and P-selectin.[42,43] For instance, TNFα and IL-1β increase P-selectin synthesis in mouse ECs but not in human.[31] Moreover, immune trafficking events are difficult to observe at high spatiotemporal resolution in mouse models. 2D *in vitro* systems, including the parallel plate flow chamber or the Boyden chamber, can be cultured with human cells, but they lack 3D tissue architecture and cannot simulate all of the steps of extravasation.[44] Organ-on-a-chip systems provide a convenient way to create a more comprehensive tissue architecture complete with vasculature and physiologic flows to investigate cell adhesion, extravasation/intravasation, and effector function all in the same system.[19,45,46] We have recently reported a microfluidic model of vascularized cardiac tissue appropriate to observe immune cell trafficking in the cardiac microenvironment.[18]

The COVID-19 relevant cytokine storm is characterized by elevated serum levels of many cytokines including IL-6, IL-10, IL-1β, TNFα.[22,34] Among these cytokines IL-1β and TNFα induce endothelial expression of E-selectins[40] and alter confirmation of leukocyte integrins to a high affinity state.[39] Both cytokines induce expression of E-selectin in ECs, but TNFα induces higher expression of membrane bound E-selectin and IL-1β induces higher expression of soluble E-selectin.[47] Therefore, we chose a cocktail of these two cytokines to simulate severe COVID-19 relevant cytokine storm-like conditions in our model system and demonstrated a robust accumulation of PMNs in the tissue (Fig. 4) in response to cytokine storm-like condition on the chip. The accumulation of PMNs and extravasation increased with increasing concentration of the cytokines (Fig. 4) as expected, given expression of adhesion molecules and permeability of vessels is expected to increase in response to increasing concentrations of IL-1β and TNFα treatments.[47]

In addition to E-selectin, TNFα and IL-1β elevate expression of VCAM-1 and ICAM-1 in ECs.[48–50] However, selectins extend farther from the surface and above the glycocalyx of ECs and thus are more likely to form the initial tether with a flowing cell. Therefore, DS–IkL is designed to

target E-selectin. The accumulation of PMNs (a measure of initial tethering in our assay) was robustly reduced by DS–IkL (>50%) consistent with DS–IkL is a potent blocker of E-selectin mediated tethering (Fig. 5). Once the leukocytes form the initial tether to the ECs, they exhibit rolling mediated by selectins, VCAM-1, and ICAM-1.[40] Leukocyte rolling prepares them for further steps of firm arrest and trans-endothelial migration (extravasation). Cell rolling is an exquisite phenomenon in which new bonds are formed at the leading edge of a rolling cell while the bonds at the trailing edge are broken. A cell exhibits smooth slow rolling only if the kinetics of bond formation is balanced by the bond-breakage, else the cells exhibit fast rolling. DS–IkL is designed as a large multivalent proteoglycan complex (MW ≈ 60 kDa) and can thus sterically hinder access to other adhesion molecules (VCAM-1 and ICAM-1) that have overlapping function with selectins. Our data showed smooth slow rolling of PMNs on the inflamed endothelium of the tissue-chip, but the rolling speed increased ~2-fold when the devices were treated with DS–IkL (video SV1 and SV2,† and Fig. 5). Thus, our data is consistent with the mechanism of action of DS–IkL to reduce accumulation of PMNs by inhibiting primary tethering to E-Selectin as well as the slow rolling of leukocytes mediated by VCAM-1 and ICAM-1 on the endothelium necessary for extravasation.[16]

Interestingly, the ECs in our model function as a positive feedback regulator to elevate the level of pro-inflammatory cytokines. The endothelial production of IL-6 reached physiological levels observed in cytokine storm of COVID-19 patients.[22] IFNγ in the serum of severe COVID-19 patients varies in a wide concentration range of three orders of magnitude (0.2–200 pg mL^{-1}).[34,51–53] In our model IFNγ was detectable from endothelial cells only (~1 pg ml^{-1}) on the lower side of this concentration spectrum. This observation is likely due to the myriad of additional sources of IFNγ *in vivo*; for example, the current version of the cardiac tissue-chip does not contain macrophages, which are an additional source of not only IFNγ, but additional inflammatory cytokines.[4] Furthermore, we present only a simplified version of cytokine storm-like conditions emphasizing early cytokines and those that are known to impact adhesion molecules in the endothelium (*i.e.*, TNFα and IL-1β). There are many additional cytokines (*e.g.*, IL-2, IL-10, MCP-1) involved in the cytokine storm,[1,2,4] and although we did not use these cytokines as part of our stimulus or assess the levels of these following our initial stimulus, they could impact our results.

In our model of vascularized cardiac tissue, the cytokine storm-like conditions increased spontaneous beating of cardiomyocytes consistent with the reports that cytokine storm increase cardiac arrhythmias.[54] PMN are known to secrete reactive oxygen species (ROS),[55] which can damage sarco-/endoplasmic reticulum (SER) by the SER Ca^{2+} pump (SERCA) and overload cells with Ca^{2+} and Na^{+}.[56] Spontaneous beating under cytokine storm-like conditions in our chip may be elevated *via* a similar mechanism. Finally, while a previous report has shown that TNFα and IL-1β alone can stimulate beat frequency,[57] the concentrations utilized are more than two orders of magnitude higher than that used in our study (Fig. 6) and present *in vivo* during severe COVID-19.[22]

Conclusions

In summary, we have created a vascularized cardiac tissue-chip capable of simulating features of the cytokine storm associated with COVID-19. Physiologic levels of TNFα and IL-1β, based on serum concentration of patients with COVID-19, induced the production of additional cytokines including TNFα, IL-1β, IL-6, and IFNγ; enhanced attachment and extravasation of PMNs into a cardiac tissue microenvironment; and increased the spontaneous beat rate of the cardiac tissue. The attachment and extravasation of PMNs, as well as the enhanced beat rate, were attenuated with the treatment of DS–IkL, a novel multivalent selectin-targeting carbohydrate conjugate that binds to E-selectin on the endothelium. We conclude that DS–IkL can limit PMN trafficking into inflamed tissues and may be a useful intervention to mitigate the cardiac effects of COVID-19 cytokine storm.

Conflicts of interest

There are no conflicts to declare.

Acknowledgements

The authors would like to thank Dr. Sherri M Biendarra-Tiegs and Dr. Matthew B. Curtis for technical assistance. We would also like to thank UC Davis Centre for Nano and Micro Manufacturing (CNM2), where a part of the microfabrication was performed. This work was supported by the National Institutes of Health UH3 HL141800 and HL141800-04S1.

References

1 S. F. Pedersen and Y. C. Ho, *J. Clin. Invest.*, 2020, **130**(5), 2202–2205.
2 T. Hirano and M. Murakami, *Immunity*, 2020, **52**, 731–733.
3 J. Rex, A. Lutz, L. E. Faletti, U. Albrecht, M. Thomas, J. G. Bode, C. Borner, O. Sawodny and I. Merfort, *Front. Physiol.*, 2019, **10**, 117.
4 L. Yang, X. Xie, Z. Tu, J. Fu, D. Xu and Y. Zhou, *Signal Transduction Targeted Ther.*, 2021, **6**, 255.
5 K. J. Huang, I. J. Su, M. Theron, Y. C. Wu, S. K. Lai, C. C. Liu and H. Y. Lei, *J. Med. Virol.*, 2005, **75**, 185–194.
6 M. Liao, Y. Liu, J. Yuan, Y. Wen, G. Xu, J. Zhao, L. Cheng, J. Li, X. Wang, F. Wang, L. Liu, I. Amit, S. Zhang and Z. Zhang, *Nat. Med.*, 2020, **26**, 842–844.
7 D. Wang, B. Hu, C. Hu, F. Zhu, X. Liu, J. Zhang, B. Wang, H. Xiang, Z. Cheng, Y. Xiong, Y. Zhao, Y. Li, X. Wang and Z. Peng, *JAMA*, 2020, DOI: **10.1001/jama.2020.1585**.
8 Y. Du, L. Tu, P. Zhu, M. Mu, R. Wang, P. Yang, X. Wang, C. Hu, R. Ping, P. Hu, T. Li, F. Cao, C. Chang, Q. Hu, Y. Jin and G. Xu, *Am. J. Respir. Crit. Care Med.*, 2020, **201**(11), 1372–1379.

9 Q. Ruan, K. Yang, W. Wang, L. Jiang and J. Song, *Intensive Care Med.*, 2020, **46**(5), 846–848.
10 C. I. Wu, P. G. Postema, E. Arbelo, E. R. Behr, C. R. Bezzina, C. Napolitano, T. Robyns, V. Probst, E. Schulze-Bahr, C. A. Remme and A. A. M. Wilde, *Heart Rhythm.*, 2020, **17**(9), 1456–1462.
11 S. Shi, M. Qin, B. Shen, Y. Cai, T. Liu, F. Yang, W. Gong, X. Liu, J. Liang, Q. Zhao, H. Huang, B. Yang and C. Huang, *JAMA Cardiol.*, 2020, **5**(7), 802–810.
12 L. Villaescusa, F. Zaragozá, I. Gayo-Abeleira and C. Zaragozá, *Adv. Ther.*, 2022, 1–23.
13 S. R. Barthel, J. D. Gavino, L. Descheny and C. J. Dimitroff, *Expert Opin. Ther. Targets*, 2007, **11**, 1473–1491.
14 I. Mitroulis, V. I. Alexaki, I. Kourtzelis, A. Ziogas, G. Hajishengallis and T. Chavakis, *Pharmacol. Ther.*, 2015, **147**, 123–135.
15 V. R. Muzykantov, *ISRN Vasc. Med.*, 2013, **2013**, 916254.
16 T. Dehghani, P. N. Thai, H. Sodhi, L. Ren, P. Sirish, C. E. Nader, V. Timofeyev, J. L. Overton, X. Li, K. S. Lam, N. Chiamvimonvat and A. Panitch, *Cardiovasc. Res.*, 2022, **118**, 267–281.
17 M. L. Moya, Y. H. Hsu, A. P. Lee, C. C. Hughes and S. C. George, *Tissue Eng., Part C*, 2013, **19**, 730–737.
18 K.-C. Weng, Y. K. Kurokawa, B. S. Hajek, J. A. Paladin, V. S. Shirure and S. C. George, *Tissue Eng., Part C*, 2020, **26**, 44–55.
19 D. E. Glaser, M. B. Curtis, P. A. Sariano, Z. A. Rollins, B. S. Shergill, A. Anand, A. M. Deely, V. S. Shirure, L. Anderson, J. M. Lowen, N. R. Ng, K. Weilbaecher, D. C. Link and S. C. George, *Biomaterials*, 2022, **280**, 121245.
20 V. S. Shirure, A. Lezia, A. Tao, L. F. Alonzo and S. C. George, *Angiogenesis*, 2017, **20**, 493–504.
21 Y. Bi, V. S. Shirure, R. Liu, C. Cunningham, L. Ding, J. M. Meacham, S. P. Goedegebuure, S. C. George and R. C. Fields, *Integr. Biol.*, 2020, **12**, 221–232.
22 D. M. Del Valle, S. Kim-Schulze, H.-H. Huang, N. D. Beckmann, S. Nirenberg, B. Wang, Y. Lavin, T. H. Swartz, D. Madduri, A. Stock, T. U. Marron, H. Xie, M. Patel, K. Tuballes, O. Van Oekelen, A. Rahman, P. Kovatch, J. A. Aberg, E. Schadt, S. Jagannath, M. Mazumdar, A. W. Charney, A. Firpo-Betancourt, D. R. Mendu, J. Jhang, D. Reich, K. Sigel, C. Cordon-Cardo, M. Feldmann, S. Parekh, M. Merad and S. Gnjatic, *Nat. Med.*, 2020, **26**, 1636–1643.
23 J.-M. Li, L. M. Fan, M. R. Christie and A. M. Shah, *Mol. Cell. Biol.*, 2005, **25**, 2320–2330.
24 H. S. Sakhalkar, M. K. Dalal, A. K. Salem, R. Ansari, J. Fu, M. F. Kiani, D. T. Kurjiaka, J. Hanes, K. M. Shakesheff and D. J. Goetz, *Proc. Natl. Acad. Sci. U. S. A.*, 2003, **100**, 15895–15900.
25 V. S. Shirure, N. M. Reynolds and M. M. Burdick, *PLoS One*, 2012, **7**, e44529.
26 M. L. Moya, L. F. Alonzo and S. C. George, *Methods Mol. Biol.*, 2014, **1202**, 21–27.
27 X. Lian, C. Hsiao, G. Wilson, K. Zhu, L. B. Hazeltine, S. M. Azarin, K. K. Raval, J. Zhang, T. J. Kamp and S. P. Palecek, *Proc. Natl. Acad. Sci. U. S. A.*, 2012, **109**, E1848–1857.
28 S. M. Biendarra-Tiegs, S. Yechikov, B. Shergill, B. Brumback, K. Takahashi, V. S. Shirure, R. E. Gonzalez, L. Houshmand, D. Zhong, K.-C. Weng, J. Silva, T. W. Smith, S. L. Rentschler and S. C. George, *Physiol. Rep.*, 2022, **10**, e15407.
29 J. R. Wodicka, V. A. Morikis, T. Dehghani, S. I. Simon and A. Panitch, *Cell. Mol. Bioeng.*, 2019, **12**, 121–130.
30 B. J. Ballermann, A. Dardik, E. Eng and A. Liu, *Kidney Int.*, 1998, **54**, S100–S108.
31 N. Baeyens, C. Bandyopadhyay, B. G. Coon, S. Yun and M. A. Schwartz, *J. Clin. Invest.*, 2016, **126**, 821–828.
32 T. Hompland, C. Ellingsen, K. M. Ovrebo and E. K. Rofstad, *Cancer Res.*, 2012, **72**, 4899–4908.
33 J. M. Rutkowski and M. A. Swartz, *Trends Cell Biol.*, 2007, **17**, 44–50.
34 A. C. Gadotti, M. de Castro Deus, J. P. Telles, R. Wind, M. Goes, R. G. C. Ossoski, A. M. de Padua, L. de Noronha, A. Moreno-Amaral, C. P. Baena and F. F. Tuon, *Virus Res.*, 2020, **289**, 198171.
35 Y. K. Kurokawa, R. T. Yin, M. R. Shang, V. S. Shirure, M. L. Moya and S. C. George, *Tissue Eng., Part C*, 2017, **23**, 474–484.
36 Y. Zheng, J. Chen, M. Craven, N. W. Choi, S. Totorica, A. Diaz-Santana, P. Kermani, B. Hempstead, C. Fischbach-Teschl, J. A. Lopez and A. D. Stroock, *Proc. Natl. Acad. Sci. U. S. A.*, 2012, **109**, 9342–9347.
37 B. Marcos-Ramiro, D. García-Weber and J. Millán, *Thromb. Haemostasis*, 2014, **112**, 1088–1102.
38 S. Kerkar, M. Williams, J. M. Blocksom, R. F. Wilson, J. G. Tyburski and C. P. Steffes, *J. Surg. Res.*, 2006, **132**, 40–45.
39 M. Lourda, M. Dzidic, L. Hertwig, H. Bergsten, L. M. Palma Medina, I. Sinha, E. Kvedaraite, P. Chen, J. R. Muvva, J.-B. Gorin, M. Cornillet, J. Emgård, K. Moll, M. García, K. T. Maleki, J. Klingström, J. Michaëlsson, M. Flodström-Tullberg, S. Brighenti, M. Buggert, J. Mjösberg, K.-J. Malmberg, J. K. Sandberg, J. I. Henter, E. Folkesson, S. Gredmark-Russ, A. Sönnerborg, L. I. Eriksson, O. Rooyackers, S. Aleman, K. Strålin, H.-G. Ljunggren, N. K. Björkström, M. Svensson, A. Ponzetta, A. Norrby-Teglund, B. J. Chambers and Karolinska KI/K COVID-19 Study Group, *Proc. Natl. Acad. Sci. U. S. A.*, 2021, **118**(40), e2109123118.
40 K. Ley, C. Laudanna, M. I. Cybulsky and S. Nourshargh, *Nat. Rev. Immunol.*, 2007, **7**, 678–689.
41 C. Hartmann, A. F. R. D. S. Miggiolaro, J. da S. Motta, L. B. Carstens, C. B. V. De Paula, S. F. Grobe, L. H. de Souza Nunes, G. L. Marques, P. Libby, L. Z. Moura, L. de Noronha and C. P. Baena, *Front. Immunol.*, 2021, **12**, 748417.
42 L. Yao, H. Setiadi, L. Xia, Z. Laszik, F. B. Taylor and R. P. McEver, *Blood*, 1999, **94**, 3820–3828.
43 Z. Liu, J. J. Miner, T. Yago, L. Yao, F. Lupu, L. Xia and R. P. McEver, *J. Exp. Med.*, 2010, **207**, 2975–2987.
44 W. A. Muller and F. W. Luscinskas, *Methods Enzymol.*, 2008, **443**, 155–176.
45 K. H. Benam, R. Villenave, C. Lucchesi, A. Varone, C. Hubeau, H.-H. Lee, S. E. Alves, M. Salmon, T. C. Ferrante, J. C. Weaver, A. Bahinski, G. A. Hamilton and D. E. Ingber, *Nat. Methods*, 2016, **13**, 151–157.

46 V. S. Shirure, C. C. W. Hughes and S. C. George, *Annu. Rev. Biomed. Eng.*, 2021, **23**, 141–167.
47 V. Mako, J. Czucz, Z. Weiszhar, E. Herczenik, J. Matko, Z. Prohaszka and L. Cervenak, *Cytometry, Part A*, 2010, **77**, 962–970.
48 C. L. Myers, S. J. Wertheimer, J. Schembri-King, T. Parks and R. W. Wallace, *Am. J. Physiol.*, 1992, **263**, C767–C772.
49 D. Wong and K. Dorovini-Zis, *Microvasc. Res.*, 1995, **49**, 325–339.
50 M. Sans, J. Panes, E. Ardite, J. I. Elizalde, Y. Arce, M. Elena, A. Palacin, J. C. Fernandez-Checa, D. C. Anderson, R. Lobb and J. M. Pique, *Gastroenterology*, 1999, **116**, 874–883.
51 P.-K. Chen, K.-J. Yeo, S.-H. Chang, T.-L. Liao, C.-H. Chou, J.-L. Lan, C.-K. Chang and D.-Y. Chen, *Virol. J.*, 2023, **20**, 33.
52 W. Luo, J.-W. Zhang, W. Zhang, Y.-L. Lin and Q. Wang, *J. Med. Virol.*, 2021, **93**, 89–91.
53 M. Y. Merza, R. A. Hwaiz, B. K. Hamad, K. A. Mohammad, H. A. Hama and A. Y. Karim, *PLoS One*, 2021, **16**, e0250330.
54 P. E. Lazzerini, F. Laghi-Pasini, M. Boutjdir and P. L. Capecchi, *Nat. Rev. Immunol.*, 2022, **22**, 270–272.
55 F. Carbone, A. Nencioni, F. Mach, N. Vuilleumier and F. Montecucco, *Thromb. Haemostasis*, 2013, **110**, 501–514.
56 J. Pande and A. K. Grover, in *Systems Biology of Free Radicals and Antioxidants*, ed. I. Laher, Springer Berlin Heidelberg, Berlin, Heidelberg, 2014, pp. 1077–1090.
57 C. V. Oddis, R. L. Simmons, B. G. Hattler and M. S. Finkel, *Biochem. Biophys. Res. Commun.*, 1994, **205**, 992–997.